AMINE-GRAFTED MESOPOROUS SILICA FOR CO_2 CAPTURE

R. SERRANO†, P. CUESTA ZAPATA‡, E.GONZO§ and M.PARENTIS§

†*INIQUI, CONICET, Univ. Nac. de Salta, 4400 Salta, Argentina*
roserrano1988@gmail.com
‡ *Fac. de Cs. Exactas - INIQUI, Univ. Nac. de Salta, 4400 Salta, Argentina*
pcuesta@unsa.edu.ar
§ *Fac. de Ingeniería – INIQUI, Univ. Nac. de Salta, 4400 Salta, Argentina*
gonzo@unsa.edu.ar, mparentis@unsa.edu.ar

***Abstract*— Three-aminopropyltriethoxysilane modified MCM-41 mesoporous silicas were synthesized by grafting the organic groups on the support surface, using different molar ratios of SiO_2: Aminosilane. The synthesized solids were characterized by N_2 adsorption, XRD, FTIR and TG-DTA. MCM-41 has a specific surface area of about 1500 m^2/g, while that of the functionalized materials falls around 600 m^2/g, showing a tendency to decrease as the content of the functionalizing agent grows. The N_2 adsorption isotherms of pure and functionalized materials are characteristic of mesoporous type IV materials. The structural properties were studied by FTIR and XRD. TG-DTA studies allow analyzing the thermal stability of the materials and determining the deposited amine content. The aminosilane modified mesoporous silica materials increase the CO_2 adsorption capacity compared to that of the pure support. Freundlich, Dual Sites Sips and Dubinin-Radushkevich equation models, all explained data satisfactorily. Further analysis using Freundlich equation revealed that the model parameters showed linear correlation with APTES molar content in the samples.**

***Keywords*—MCM-41, APTES, Grafting, Carbon dioxide adsorption, Freundlich model.**

I. INTRODUCTION

Carbon dioxide is a major anthropogenic greenhouse gas, contributing to the global warming in more than 60%. About 40% of the current CO_2 emissions in the world have been emitted from power generation plants (IEA, 2017). Because fossil fuels will keep on being the main source of primary energy in the next few decades, the development of an effective means to capture CO_2 from the flue gases of power generation plants is essential in order to contribute with the worldwide demand of CO_2 reduction.

Currently, CO_2 captures involve chemisorption on alkylamine liquids, resulting in carbamate under anhydrous conditions, followed by a conversion into carbonate or bicarbonate salts in water (Chen and Bhattacharjee, 2017; Sanz-Pérez *et al.*, 2018; Zhang *et al.*, 2017). This method has several disadvantages, such as high-energy consumption to regenerate the liquids, equipment corrosion, high viscosity and solvent degradation (Zhang *et al*., 2017).

To remedy the problems, studies of sorption-based technologies and processes, usually involving solid CO_2 adsorbents, have attracted considerable interest (Sanz-Pérez *et al*., 2018; Zukal *et al*., 2018). CO_2 adsorbents are mainly porous materials, such as zeolites (Sarker *et al*., 2017; Ullah *et al.*, 2018; Zukal *et al*., 2018), porous carbon (Sarker *et al*., 2017; Singh *et al*., 2018; Zhang *et al*., 2015), and metal-organic frameworks (MOFs) (Ahmed and Jhung, 2017; Hu *et al*., 2018; Qasem *et al.*, 2018). These materials usually have large surface area (micropores) and capture CO_2 by physical adsorption. Compared to liquid amine absorption, they have significant advantages for energy efficiency. On the other hand, they also suffer from drawbacks, such as low CO_2 capture selectivity and poor performance under moisture conditions. In particular, mesoporous materials such as MCM-41, SBA-15 and MCF are promising as adsorbents for CO_2 capture (Kumar *et al.*, 2014; Schell *et al.*, 2012), although the selectivity of these adsorbents is low since such adsorption is a physical interaction rather than a chemical one. Incorporating amine species into the porous structure to form an organic-inorganic hybrid compound for CO_2 capture has also attracted increasing attention (Chen *et al.*, 2017; Loganathan and Ghoshal, 2017; Zhang *et al.*, 2017). The composite combines the advantages of both amine species (high CO_2 affinity) and porous materials (large surface area and large pore volume) through the homogeneous distribution of amine species inside a stable porous structure.

There are two main classes of such adsorbent materials: (a) amines covalently bound to the silica support (Chen *et al*., 2017; Loganathan and Ghoshal, 2017; Zhang *et al.*, 2017) via the use of silane chemistry and (b) liquid amines like polyethyleneimine (PEI) physically impregnated into the silica support by "wet impregnation" method (Chen *et al*., 2017; Xu *et al*., 2002). Xu et al. modified a mesoporous molecular sieve of MCM-41 type with polyethylenimine with different amounts of polymer in the range between 15 – 75 w%. They found that the mesoporous molecular sieve had a synergetic effect on the adsorption of CO_2 by PEI. A CO_2 adsorption capacity of 2.4 mmol-CO_2/g-adsorbent was obtained with MCM-41-PEI-50 w% at 75 °C.

The aim of this study is to synthesize 3-aminopropyl modified MCM-41 by the post synthesis grafting method, via the use of silane chemistry. A subsequent characterization of the textural, structural and thermal stability properties, as well as the CO_2 adsorption capacity, are carried out. The adsorption phenomenon is interpreted with several appropriate model equations. The effects of

the silylation agent content on the adsorption capacity and on the model parameters are also analyzed.

II. METHODS

A. Synthesis

A.1 Synthesis of MCM-41

The procedure used for the synthesis was previously reported by Grün *et al.* (1999), using n-hexadecyltrimethylammonium bromide (CTAB) as template and tetraethoxysilane (TEOS) as a source of silica. The TEOS: CTAB: NH_3: H_2O molar composition was 1: 0.15: 2.8: 141.2. The material was filtered, washed and dried at 90°C for 12 hours. The surfactant was removed by calcination at 550°C. This material is denoted as M23.

A.2 Functionalization of MCM-41 by APTES

Aminopropyl-modified MCM-41 samples were synthesized by reaction of calcined MCM-41 (1 g) and APTES in 15 mL of toluene under reflux and N_2 atmosphere. The reaction temperature was 95ºC and the amount of APTES added was such that the SiO_2: APTES molar ratio of the different samples was: 1: 0.1; 1: 0.15; 1: 0.2 and 1: 0.5 (M23+0.1; M23+0.15; M23+0.2 and M23+0.5, respectively). After treatment, the solids were removed by vacuum filtration and washed with ethanol and water.

B. Characterization

B.1. Textural characterization:

Adsorption - desorption isotherms were carried out in a Micromeritics ASAP-2020 sorptometer, employing N_2 as the adsorbent. The specific surface area was calculated using the standard BET method on the basis of adsorption data in a relative pressure range from 0.05-0.35. The pore size distributions were calculated from adsorption branches of the isotherms using the BJH method.

B.2. X-Ray Diffraction (DRX): Crystallography studies and the mesoporous array of the samples were carried out in a Phillips-PW-1700 powder diffractometer with a monochromatized CuKα radiation.

B.3. Fourier Transform Infrared spectroscopy (FTIR): The FTIR spectra were recorded on a Spectrum GX-FTIR Perkin Elmer spectrophotometer. The absorption spectra were obtained from the samples diluted with KBr and pressed at 2 Tn/cm^2. The spectra were normalized to the height of the SiO_4 band at the 1150 -1000 cm^{-1} region.

B.4. Thermo-gravimetric (TG) and differential thermal analysis (DTA): The TG and DTA analysis were carried out in air, in a RIGAKU unit, at a heating rate of 10°C/min, from room temperature to 1000°C. The amount of sample was 15 mg approximately.

C. CO_2 Adsorption Experiments

The adsorption measurements were performed on a Cahn D 200 electrobalance, which is connected to a high vacuum unit. The equipment sensor allows registering the sorbed mass with a sensitivity of 1 μg, under pressure and temperature controlled conditions. The samples were previously treated under vacuum at 190ºC for 1 h. Then, the isotherms were carried out at a temperature of 25ºC for the pure support and the functionalized materials, introducing pure CO_2 in the pressure range of 0-660 mmHg, verifying that the equilibrium was reached before each measurement.

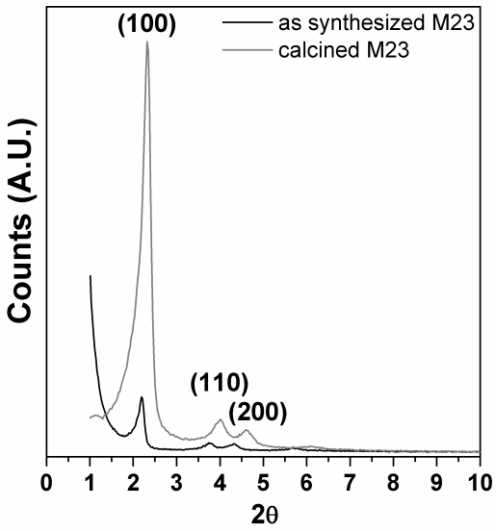

Figure 1: DRX of calcined M23 and as synthesized M23

III. RESULTS AND DISCUSSION

A. Characterization

The XRD patterns of MCM-41 before surfactant removal and after calcination at 550°C are reported in Fig. 1. Three different peaks of XRD patterns of the as-synthesized MCM-41 that can be indexed to (100), (110) and (200) reflections (2θ values of 2.2, 3.7 y 4.3 respectively), corresponding to characteristics of hexagonal and highly ordered structure in MCM-41 can be seen (Grün *et al*., 1999; Joseph *et al*., 2007).

After template removal, the XRD intensity of peak at (100) of calcined MCM-41 was greater than the as-synthesized MCM-41. Two additional peaks with low intensities at (110) and (200) reflections, at 2θ values of 4.0 y 4.6, can also be seen. The increasing intensity of the calcined MCM-41 is attributed to the presence of small and well defined pores obtained after the surfactant removal.

Table 1 shows the textural properties of the synthesized materials. The pure mesostructured material (M-23) has a high specific surface area of about 1500 m^2/g.

Amine modified MCM-41 sample, with a SiO_2: APTES molar ratio of 1: 0.1, leads to a significant decrease in BET specific surface area (about 56%). Further increases in APTES content lead to a slight and progressive decrease of BET surface. Regarding the pores volume, the introduction of the organic fragment leads to a drop of this parameter.

The N_2 adsorption isotherms on MCM-41 and aminopropyl-modified MCM-41, with different content of functionalizing agent, are shown in Fig. 2-a). All the samples show type IV isotherms, characteristic of mesoporous materials.

The isotherm of the unmodified material exhibits a volume increase, at $P/P_0 < 0.1$ values, attributed to the monolayer-multilayer N_2 adsorption on the walls of the

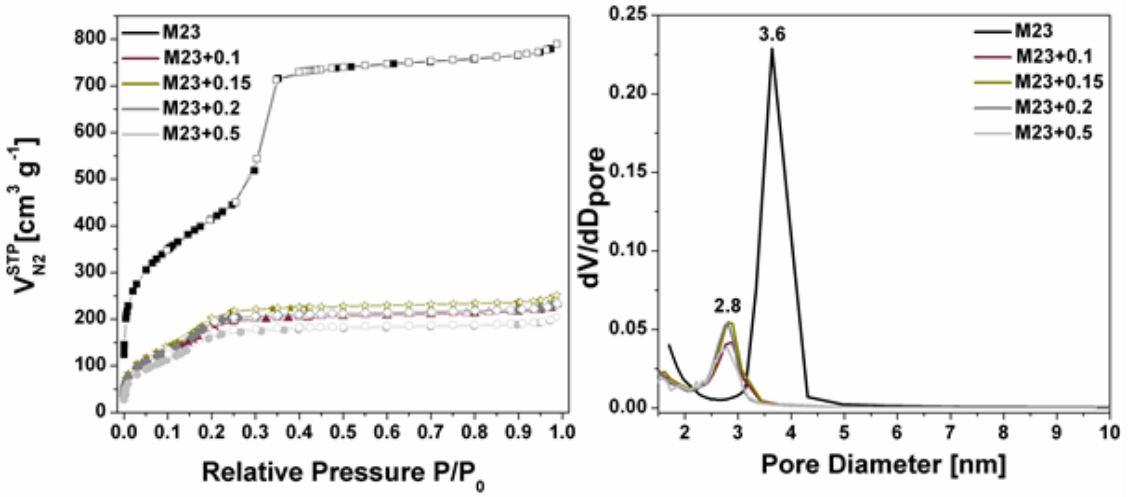

Figure 2: a) N_2 adsorption isotherms, b) pore size distribution of MCM-41 and aminopropyl-modified MCM-41

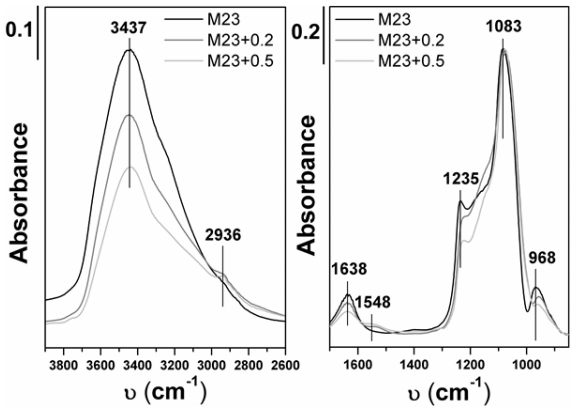

Figure 3: FTIR of pure and modified MCM-41. a) 4000 – 2400 cm^{-1}. b) 1750 – 850 cm^{-1}

Table 1: Textural properties of the materials.

Adsorbent	Molar Ratio SiO_2:APTES	S_{BET} (m^2/g)	D_p (nm)	V_{STP}* (cm^3g^{-1})
M-23	1	1505	3.6	1.21
M23+0.1	1:0.1	661	2.9	0.36
M23+0.15	1:0.15	645	2.8	0.38
M23+0.2	1:0.2	616	2.8	0.36
M23+0.5	1:0.5	539	2.8	0.31

*According to Gurvich

mesopores. Then it shows a pronounced increase in volume associated with capillary condensation in the narrow pore size, in the 0.25 to 0.35 range. The isotherm is reversible and shows no hysteresis. After amine functionalization the change in volume moves downwards and becomes even broader, indicating a decrease in the mean pore diameter. The modified samples show a small hysteresis loop associated with capillary condensation. Figure 2-b) shows the pore size distribution of pure and modified samples. The average pore diameter of the modified samples is lower than that corresponding to pure MCM-41 (3.6 nm) due to the adhesion of the aminosilane molecules on the wall of the support pores, decreasing to 2.8 nm.

Figure 3 shows the infrared spectra of pure MCM-41 and aminosilane modified MCM-41. In the 4000–2400 cm^{-1} spectral region (Fig. 3-a),the band corresponding to the O-H stretching vibrations in the presence of hydrogen bridge bonds is observed at 3437 cm^{-1}. The intensity of this band decreases when greater APTES contents are incorporated. Furthermore, the functionalized samples show a band at 2936 cm^{-1} attributed to the C-H stretching vibrations of the aminopropyl groups anchored on the surface of the support (Szegedi *et al*., 2011).

In the 1700–900 cm^{-1} spectral region (Fig. 3-b), the spectrum of pure support shows a main band at 1083 cm^{-1}, with a shoulder around 1235 cm^{-1} assigned respectively to transversal optical and longitudinal optical asymmetric stretching modes of Si-O-Si (Al-Oweini and El-Rassy, 2009). In addition, the modified samples present a band at 1548 cm^{-1} attributed to N-H scissoring flexions of propylamine groups, which indicates that the anchoring of the organic group has taken place (Szegedi *et al*., 2011). Finally, the band assigned to the Si-OH vibrations moves from 968 to 956 cm^{-1}, due to the interactions of the amino groups (NH_2) with the silanol groups (Si-OH) through hydrogen bonding (Szegedi *et al*., 2011).

Figure 4 shows TG curves of pure support and amine modified-MCM-41 samples with different SiO_2:APTES molar ratios, in an air atmosphere. The TG curve of calcined MCM-41 shows only an endothermic process, centered at 75°C, associated with a weight loss of 9%, due to desorption of physisorbed water. Subsequently, a smooth and continuous weight loss is observed up to 1000ºC, attributed to the dehydroxylation of the silica network. The TG curves of the modified samples show three-stage weight loss: the first endothermic step up to 200ºC is due to desorption of water, the second exothermic step between 200 – 500ºC, is attributed to decomposition of amines anchored to the pore wall of mesoporous MCM-41 and the third weight loss, above 500ºC, is due to dehydroxylation of surface silanols groups (Vunain *et al.*, 2014).

Table 2 reports the weight loss corresponding to stage 2 (WL_2) and the total weight loss (WL_{Total}) of all functionalized samples. Thus, the number of organosilane molecules adhering per 1 nm^2 of MCM-41 surface area (denoted as N) and the amine content defined as the num-

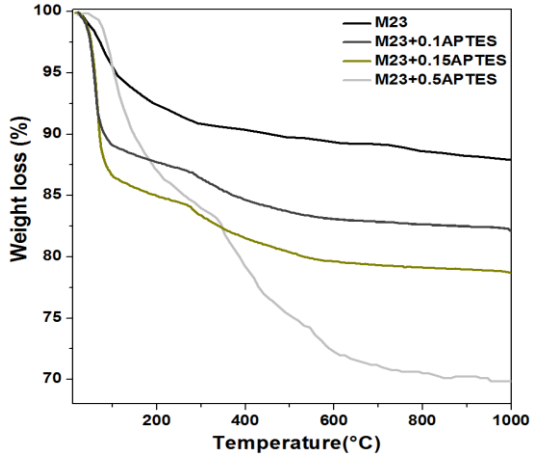

Figure 4: TG curves of pure and amine modified MCM-41 samples.

Table 2: Amine content per unit area (N) and per gram of adsorbent (CA).

Adsorbent	Weight loss of stage 2 (%)	Total weight loss(%)	N	CA
M23 + 0,1	4.6	17.75	0.88	0.96
M23+ 0,15	5	20.8	1.02	1.09
M23 + 0,5	12.4	30.5	3.44	3.08

N = organosilane molecules per nm^2 of surface area.
CA= mmoles N per gram of adsorbent.

ber of Nitrogen atoms (mmoles) per 1 gram of adsorbent (denoted as CA), were estimated by TG analysis. The calculations of N and CA were based on Eq. 1 and 2 and the results obtained are reported in Table 2. It can be seen that both N and CA grow as the APTES content in the synthesis gel increases.

$$N = \frac{WL_2}{(100-WL_{Total})} \frac{N_{Av}}{MW.S_{BET}.10^{18}} \quad (1)$$

$$CA = \frac{WL_2}{(100-WL_{Total})} \frac{1.10^3}{MW} \quad (2)$$

where MW is the Aminopropyl group molecular weight and N_{Av} is the Avogadro`s number.

B. CO_2 Adsorption

B.1. Experimental Results

Figure 5 shows the CO_2 adsorption isotherm at 25ºC for pure and amine modified MCM-41 samples.

The CO_2 adsorption isotherm at 25ºC, for the non-functionalized support, shows an almost linear increase in the amount of CO_2 adsorbed with the pressure, suggesting the existence of weak adsorbent-adsorbate interactions. The anchoring of the amino groups on the silica surface causes changes in the shape of the isotherms, observing at low pressures (< 120 mmHg) a pronounced increase of the amount adsorbed CO_2 in relation to the support, which is attributed to the existence of strong adsorption sites, linked to the presence of amines. On the other hand, the gradual increase in the amount of gas adsorbed above 120 mmHg is attributed to physically adsorbed CO_2 on the MCM-41 material.

From the data in Figure 5, it is possible to determine the experimental CO_2 adsorption capacities at 120 mmHg and 650 mmHg at 25 ºC, of the support and functionalized samples. The results corroborate the increase of the

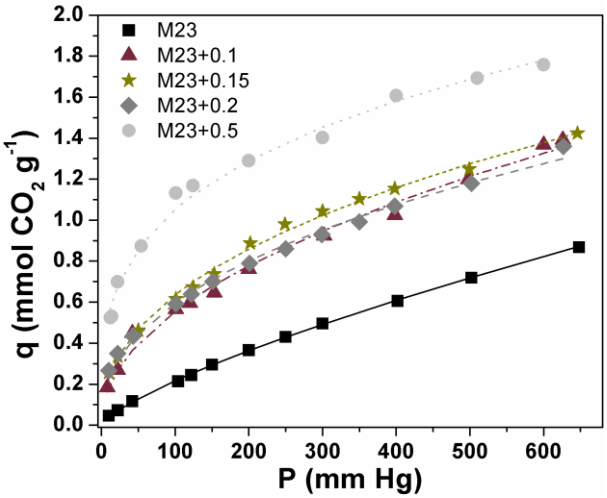

Figure 5: CO_2 adsorption isotherms at 25ºC for pure and amine modified MCM-41 samples. Experimental data (filled dots) and fitting to Freundlich model (lines).

adsorption capacity after APTES incorporation. It can be seen that, at 120 mmHg, the amount of CO_2 adsorbed from the sample with the highest APTES content is 5 times greater than that of the pure support, while at high pressures (650 mmHg) only duplicates the value corresponding to non-modified MCM-41. This observation reinforces the idea that, at low pressures, the strongest adsorption sites are first covered. Adsorption efficiency (E), defined as mmol CO_2/mmol N, at 25ºC and at 120 mmHg is 0.6 at low aminopropyl contents. This value is slightly higher than the stoichiometric value of 0.5 based on carbamate formation under dry conditions (Harlick and Sayari, 2007). At higher amine contents (M23 + 0.5), the efficiency falls to values of around 0.4.

The CO_2 adsorption capacities of the synthesized samples are within the range of those reported in the literature. However, our synthesized material has a similar adsorption capacity despite having a smaller amount of anchored aminopropyl species than other mesostructured adsorbents (Barbosa *et al*., 2011 and Vilarrasa-García *et al*., 2015).

B.2. Modeling of the Isotherms

The Freundlich, Dual Sites Sips and Dubinin-Radushkevich models were employed for modeling the adsorption isotherms of the pure support and functionalized samples. The best procedure for fitting the model with experimental data is by carrying out a nonlinear regression analysis using Polymath 5.1 program.

The Freundlich equation:

$$q = K.P^{1/n} \quad \text{with} \quad n = \frac{-\Delta H_{ad}}{R.T} \quad (3)$$

where K is a constant related to the adsorption capacity and n is a constant linked to the adsorption heat, gives satisfactory results for fitting experimental data (Fig. 5). Thus, K and n model parameters were determined and their values reported in Table 3, for samples grafted with different amine contents.

It can be seen that K is an order of magnitude smaller for the support than for the functionalized samples. For

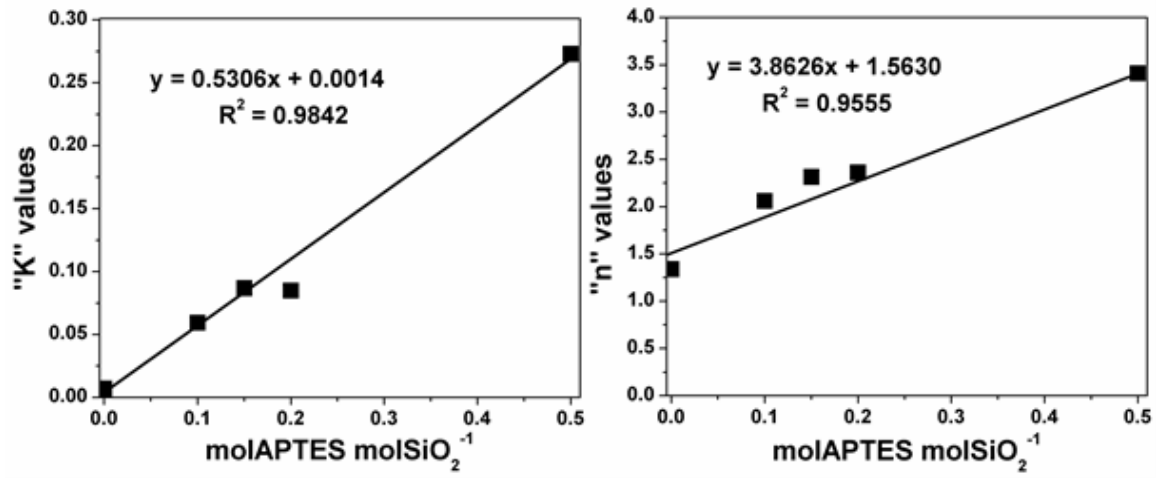

Figure 7: Variation of K values (left) and n values (right) with APTES molar content.

Table 3. Freundlich isotherms constants of CO_2 adsorption onto MCM-41and amine modified MCM-41

Adsorbent	*K*	*n*	$-\Delta H_{ad}$ (*KJ/mol*)	R^2
M23	0.0070	1.35	3.34	0.9997
M23+0.1	0.0594	2.06	5.10	0.9905
M23+0.15	0.0869	2.31	5.72	0.9964
M23+0.2	0.0849	2.36	5.85	0.9933
M23+0.5	0.2730	3.41	8.45	0.9912

the latter, as APTES content grows in the gel, the *K* values increased. On the other hand, *n*, linked to the adsorption heat (Gonzo, 2011), presents a lower value for pure MCM-41 than that shown for the anchored samples, which is attributed to the lower adsorbate-adsorbent interaction for pure support.

Finally, *K* and *n* parameters show a linear correlation with the APTES content in the material, as can be seen in Fig. 7, which gives a greater support to the application of Freundlich model.

The invariability of the thermodynamic properties with the coverage degree, such as the adsorption heat, involves the presence of uniform surfaces, which generally respond to the Langmuir Model. The modification of the adsorption heat with APTES molar content, determined at 25°C, denotes non-uniformity in the activity of the CO_2 adsorption sites. This means that the most active centers will adsorb CO_2 more strongly, generating a greater adsorption enthalpy change, which decreases as active sites have less activity. This behavior has been observed in systems that can be fitted with the Temkin model for chemical adsorption and the Freundlich model for both physical and chemical adsorption.

Sips model combines Langmuir and Freundlich isotherms models describing the heterogeneity of the adsorbent surface. Dual Sites Sips Model is applied in this work in order to model chemisorption sites (1) consisting in aminopropyl groups and physisorption sites (2) consisting of silanol groups and/or hydroxyl groups:

$$q = \frac{q_{m1}.(K_1.P)^{1/n1}}{1+(K_1.P)^{1/n1}} + \frac{q_{m2}.(K_2.P)^{1/n2}}{1+(K_2.P)^{1/n2}} \quad (4)$$

where q_{m1} and q_{m2} (mmol CO_2 g^{-1}) represents the maximum adsorption capacities of each type of site, K_1 and K_2 the chemisorption and physisorption equilibrium constants respectively ($mmHg^{-1}$), P is the pressure (mmHg) and n is a heterogeneity coefficient (when $n = 1$, the Sips model reduces to the Langmuir model).

Vieira *et al.* (2018) applied Sips equation to model N_2 y CH_4 adsorption and Dual Sites Sips Model in the case of CO_2 adsorption on polyamine-grafted magadiite. They found a good fitting, however they do not report the parameter values.

In the present paper, non-linear regression analysis was used to determine the isotherms constants. The maximum adsorption capacities (q_{m1}) for functionalized samples, ranging from 0.67 to 1.46 mmol CO_2 g^{-1} for increasing aminopropyl contents, are similar to the experimental adsorption capacities at 25 ° C and 120 mmHg (Fig. 5), linked to chemisorption sites at this low pressure. Modeling of the adsorption isotherms shows constancy of K_1 and K_2 values for all the samples studied, with average mean values of 0.0353 (Standard error SE=$1.0889.10^{-3}$) and $3.3255.10^{-4}$ (SE= $7.070.\ 10^{-5}$) respectively, with K_1 two orders of magnitude greater than K_2, according to the strength of the adsorbate-adsorbent interaction. Finally, n_1 and n_2 values show the presence of heterogeneous chemisorption sites (n_1>1) and more uniform physisorption sites (n_2<1).

In order to compare the micropore volume with that determined by nitrogen adsorption at -196 °C and adsorption energy with the adsorption heat derived from the Freundlich isotherm, the adsorption data were interpreted using the Dubinin-Radushkevich (D-R) equation (Romero *et al.*, 2003):

$$q = q_m^0.\exp(-B.\varepsilon^2) \quad (5)$$

where q_m^0 is the maximum amount of adsorbate that can be adsorbed in the adsorbent micropores and B is a constant related to the characteristic adsorption energy (E_{ad}) for a particular adsorbent–adsorbate system. The relationship between E_{ad} and B is:

$$E_{ad} = (2.B)^{-1/2} \quad (6)$$

The adsorption potential (ε) for gas adsorption is:

$$\varepsilon = R.T.ln\left(\frac{1}{a_e}\right) = R.T.ln\left(\frac{P_s}{P_e}\right) \quad (7)$$

Table 4. ω_0 and E_{ad} values determined from D-R Eq.

Adsorbent	ω_0 (cm^3/g)	V_{MICRO} (cm^3/g)	V_{MESO} (cm^3/g)	E_{ad} (KJ/mol)
M23	0.1980	0.22	0.90	6.54
M23+0.1	0.1863	0.06	0.23	8.39
M23+0.15	0.1738	0.09	0.24	8.91
M23+0.2	0.1556	0.08	0.24	9.05
M23+0.5	0.1705	0.06	0.20	11.18

where R= 8.31442.10^{-3} KJ/(mol.K), T=298K, a_e is CO_2 equilibrium activity, P_e CO_2 equilibrium pressure and P_s, CO_2 saturation pressure at 298K.

$$\varepsilon = 2.4777.ln\left(\frac{48480.4}{P_e}\right) \quad (8)$$

According to Dubinin's Theory of Volume Filling of Micropores (Wood, 2001), the maximum micropore volume ω_0 accessible to the adsorbate can be obtained by multiplying q_m^0 by the liquid molar volume (V_M) of the adsorbate:

$$\omega_0 = q_m^0.V_M \quad (9)$$

where V_M is 61.5 cm^3/mol.

Table 4 summarizes ω_0 and E_{ad}values determined from the characteristic parameters derived from de D-R equation. The micropore and mesopore volumes were determined from nitrogen adsorption experiments.

The maximum micropore volumes (ω_0) found from CO_2 adsorption was different than those determined via nitrogen adsorption measurements, except that of pure support (M23). The characteristic adsorption energy (E_{ad}) determined by D-R and the adsorption enthalpy determined from the Freundlich model, show the same tendency, which gives consistency to the applied models.

According to the correlation coefficient values, R^2, the goodness of fit is similar for the Freundlich model and the Dual Sites Sips equation. Meanwhile, for the D-R equation, the values of R^2 are slightly lower.

If we analyze the advantages of each model, it is important to mention the linear relationship of Freundlich parameters with APTES content and the existence of non-uniform CO_2 adsorption sites denoted by the heat of adsorption. This non-uniformity can be corroborated with the Dual Sites Sips model, which allows differentiating the chemisorption and physisorption sites and individualizing the adsorption equilibrium constants of both phenomena with great accuracy. Although the D-R equation is appropriate for micropore region analysis, this model allows us to estimate the characteristic adsorption energies, which are comparable with the adsorption enthalpy obtained from Freundlich equation.

IV. CONCLUSIONS

In this study, novel adsorbents were prepared by modification of MCM-41 with aminopropyl groups through the post-synthetic grafting process, via the use of silane chemistry.

The materials achieved have a hexagonal and highly ordered structure with nitrogen adsorption isotherms characteristic of mesoporous type IV materials. The FTIR studies allow verifying the incorporation of the organic fragment (the aminopropyl group) to the support. The thermal analysis allows determining the content of N, and therefore of aminopropyl, in the synthesized material.

APTES grafting improves the performance of this support as adsorbing agent of polluting gases, such as carbon dioxide, increasing its adsorption capacity, which grows as the content of the silylating agent increases. No destruction of the ordered mesoporous structure is observed in the range of silylating agent contents analyzed in the present work.

The Freundlich model appropriately fits the experimental data and the model parameters show a linear relationship with the molar content of the functionalizing agent present in the synthesis gel. The model can be used as a design tool for mesostructured adsorbent materials, in order to estimate the amount of APTES to be incorporated to retain a certain level of contaminating agent, as long as the functionalization process does not affect the mesoporous structure of the support.

Dual Sites Sips and Dubinin-Radushkevich Equations also show a good correlation.

REFERENCES

Ahmed, I. and Jhung, S.H. (2017). "Applications of metal-organic frameworks in adsorption/separation processes via hydrogen bonding interactions," *Chem. Eng. J.*, **310**, 197–215.

Al-Oweini, R. and El-Rassy, H. (2009). "Synthesis and characterization by FTIR spectroscopy of silica aerogels prepared using several Si(OR)4 and R″Si(OR′)3 precursors," *J. Mol. Struct.*, **919**, 140–145.

Barbosa, M.N., Araujo, A.S., Galvão, L.P.F.C., Silva, E.F.B., Santos, A.G.D., Luz, G.E. and Fernandes, V.J. (2011). "Carbon dioxide adsorption over DIPA functionalized MCM-41 and SBA-15 molecular sieves," *J. Therm. Anal. Calorim*., **106**, 779–782.

Chen, C. and Bhattacharjee, S. (2017). "Mesoporous silica impregnated with organoamines for post-combustion CO_2 capture: a comparison of introduced amine types," *Greenh. Gases Sci. Technol*., **7**, 1116–1125.

Chen, C., Zhang, S., Row, K.H. and Ahn, W.S. (2017). "Amine–silica composites for CO_2 capture: A short review," *J. Energy Chem.*, **26**, 868–880.

Gonzo, E.E. (2011). *Conceptos básicos sobre los fenómenos de transporte y transformación en catálisis heterogénea*, EUNSa. ed. EUNSa - Editorial de la Universidad Nacional de Salta, Salta

Grün, M., Unger, K.K., Matsumoto, A. and Tsutsumi, K. (1999). "Novel pathways for the preparation of mesoporous MCM-41 materials: control of porosity and morphology," *Microporous Mesoporous Mater*., **27**, 207–216.

Harlick, P.J.E. and Sayari, A. (2007). "Applications of Pore-Expanded Mesoporous Silica Triamine Grafted Material with Exceptional CO_2 Dynamic and Equilibrium Adsorption Performance," *Ind. Eng. Chem. Res*., **46**, 446-458.

Hu, J., Liu, Y., Liu, J., Gu, C. and Wu, D. (2018). "High CO_2 adsorption capacities in UiO type MOFs comprising heterocyclic ligand," *Microporous Mesoporous Mater*., **256**, 25–31.

IEA. (2017). *CO_2 Emissions from Fuel Combustion*, Int. Energy Agency.

Joseph, T., Vijay Kumar, K., Ramaswamy, A.V. and Halligudi, S.B. (2007). "Au-Pt nanoparticles in amine functionalized MCM-41: Catalytic evaluation in hydrogenation reactions," *Catal. Commun.*, **8**, 629–634.

Kumar, V., Labhsetwar, N., Drage, T., Stevens, L., Meshram, S. and Rayalu, S. (2014). "Surface Bespoke Mesoporous Silica for Carbon Dioxide Adsorption," *J. Environ. Eng.*, **140**, 04014031.

Loganathan, S. and Ghoshal, A.K. (2017). "Amine tethered pore-expanded MCM-41: A promising adsorbent for CO_2 capture," *Chem. Eng. J.*, **308**, 827–839.

Qasem, N.A.A., Ben-Mansour, R. and Habib, M.A. (2018). "An MOF-177," *Appl. Energy*, **210**, 317–326.

Romero L.C., Bonomo, A. and Gonzo, E.E., (2003). "Acid-activated Carbons from Peanut Shells: Synthesis, Characterization and Uptake of Organic Compounds from Aqueous Solutions," *Adsorption Science & Technology*, **21,** 617-626.

Sanz-Pérez, E.S., Arencibia, A., Calleja, G. and Sanz, R. (2018). "Tuning the textural properties of HMS mesoporous silica. Functionalization towards CO_2 adsorption," *Microporous Mesoporous Mater*., **260**, 235–244.

Sarker, A.I., Aroonwilas, A. and Veawab, A. (2017). "Equilibrium and Kinetic Behaviour of CO2 Adsorption onto Zeolites, Carbon Molecular Sieve and Activated Carbons," *Energy Procedia*, **114**, 2450–2459.

Schell, J., Casas, N., Blom, R., Spjelkavik, A.I., Andersen, A., Cavka, J.H. and Mazzotti, M. (2012). "MCM-41, MOF and UiO-67/MCM-41 adsorbents for pre-combustion CO_2 capture by PSA: Adsorption equilibria," *Adsorption*, **18**, 213–227.

Singh, J., Bhunia, H. and Basu, S. (2018). "CO_2 adsorption on oxygen enriched porous carbon monoliths: Kinetics, isotherm and thermodynamic studies," *J. Ind. Eng. Chem*, **60**, 321–332.

Szegedi, A., Popova, M., Goshev, I. and Mihály, J. (2011). "Effect of amine functionalization of spherical MCM-41 and SBA-15 on controlled drug release," *Solid State Chem.*, **184**, 1201–1207.

Ullah, R., Ali, H., Salah Saad, M., Aparicio, S. and Atilhan, M. (2018). "Adsorption equilibrium studies of CO_2, CH_4 and N_2 on various modified zeolites at high pressures up to 200 bars," *Microporous Mesoporous Mater*., **262**, 49–58.

Vieira, R.B., Mourab, P.A.S., Vilarrasa-García, E., Azevedo, D.C.S. and Pastore H.O. (2018). "Polyamine-Grafted Magadiite: High CO_2 Selectivity at Capture from CO_2/N_2 and CO_2/CH_4 Mixtures," *Journal of CO_2 Utilization*, **23**, 29-41.

Vilarrasa-García, E., Cecilia, J.A., Bastos-Neto, M., Cavalcante, C.L., Azevedo, D.C.S. and Rodriguez-Castellón, E. (2015). "CO_2/CH_4 adsorption separation process using pore expanded mesoporous silicas functionalizated by APTES grafting," *Adsorption*, **21**, 565–575.

Vunain, E., Opembe, N.N., Jalama, K., Mishra, A.K. and Meijboom, R. (2014). "Thermal stability of amine-functionalized MCM-41 in different atmospheres," *J. Therm. Anal. Calorim*., **115**, 1487–1496.

Wood, G.O. (2001). "Affinity Coefficientes of the Polanyi- Dubinin Adorption Isotherm Equatios: a Review with Compilations and Correlations," *Carbon*, **39**, 343-356.

Xu, X., Song, C., Andresen, J.M., Miller, B.G. and Scaroni, A.W. (2002). "Novel Polyethylenimine-Modified Mesoporous Molecular Sieve of MCM-41 Type as High-Capacity Adsorbent for CO_2 Capture," *Energy & Fuels*, **16**, 1463-1469.

Zhang, G., Zhao, P. and Xu, Y. (2017). "Development of amine-functionalized hierarchically porous silica for CO_2 capture," *J. Ind. Eng. Chem.*, **54**, 59–68.

Zhang, X.Q., Li, W.C. and Lu, A.H. (2015). "Designed porous carbon materials for efficient CO_2 adsorption and separation," *Xinxing Tan Cailiao/New Carbon Mater*., **30**, 481–501.

Zukal, A., Shamzhy, M., Kubů, M. and Čejka, J. (2018). "The effect of pore size dimensions in isoreticular zeolites on carbon dioxide adsorption heats," *J. CO_2 Util*., **24**, 157–163.

Received: May 20, 2019
Sent to Subject Editor: July 18, 2019
Accepted: February 21, 2020
Recommended by Subject Editor: Marcelo Seckler